coatings

MDPI

Article

Influence of Plasma Torch Power on the Plasma Jet Properties and Microstructure of Alumina Coatings

Airingas Šuopys [1,*], Viktorija Grigaitienė [1], Liutauras Marcinauskas [1,2], Romualdas Kėželis [1], Rolandas Uscila [1] and Mindaugas Aikas [1]

[1] Lithuanian Energy Institute, Plasma Processing Laboratory, Breslaujos str. 3, LT-44403 Kaunas, Lithuania; viktorija.grigaitiene@lei.lt (V.G.); liutauras.marcinauskas@lei.lt (L.M.); romualdas.kezelis@lei.lt (R.K.); rolandas.uscila@lei.lt (R.U.); mindaugas.aikas@lei.lt (M.A.)

[2] Department of Physics, Kaunas University of Technology, Studentų str. 50, LT-51368 Kaunas, Lithuania

* Correspondence: airingas.suopys@lei.lt

Abstract: In this study, alumina coatings were formed using atmospheric plasma spraying, increasing the torch power from 29.4 to 45.1 kW. The surface morphology of the coatings was determined using scanning electron microscopy; the elemental composition was examined using energy-dispersive X-ray spectroscopy (EDS); phase composition was investigated using X-ray diffraction; and surface roughness was determined using a profilometer. The steel surface temperature was measured using a type-K thermocouple, and the plasma jet temperature, at a distance of 70 mm, using a type-B thermocouple. Alumina particle velocity was calculated by analyzing high-speed camera footage using ImageJ software. The results indicate that plasma jet temperature, speed, and in-flight particle velocity increased with plasma torch power. Furthermore, the amount of γ-Al_2O_3 phase in the coating increased, and the α-Al_2O_3 decreased with increasing plasma power. The surface roughness (R_q) of the Al_2O_3 coatings decreased from 7.13 to 5.54 µm, with an increase in torch power. The EDS measurements indicate that the increase in torch power did not affect the elemental composition of as-sprayed coatings. The results provide a wider understanding of an atmospheric plasma spray technique, optimizing and controlling the parameters using air as a primary gas.

Keywords: plasma spraying; plasma torch; Al_2O_3; particle velocity; plasma jet temperature

Citation: Šuopys, A.; Grigaitienė, V.; Marcinauskas, L.; Kėželis, R.; Uscila, R.; Aikas, M. Influence of Plasma Torch Power on the Plasma Jet Properties and Microstructure of Alumina Coatings. *Coatings* **2022**, *12*, 934. https://doi.org/10.3390/coatings12070934

Academic Editors: Qi Hua Fan and Tomasz Dyl

Received: 13 May 2022
Accepted: 27 June 2022
Published: 1 July 2022

1. Introduction

Plasma spray technology is widely used in the manufacturing industry for the development of numerous protective coatings [1]. Atmospheric plasma spraying is a flexible, industry-scalable, and cost-effective manufacturing processing technique that has been used to deposit metallic and ceramic coatings [2]. The coatings, applied to mechanical surfaces, exhibit enhanced corrosion resistance and hardness. During the plasma coating spray process, the quality of the coatings can be widely controlled by selecting the proper spraying parameters. The structure of the deposited coatings depends on the plasma spray parameters, such as plasma jet rate, temperature, and the distance between the plasma generator outlet and the substrate [3–7]. The high temperature of the plasma jet is suitable for materials with a high melting point, e.g., ceramics [4]. In the atmospheric plasma spray process, the feedstock material is injected into the plasma jet, melted, and accelerated towards the substrate. The process is usually carried out in an open-air environment, but using a controlled atmosphere chamber is also possible. A splat is created upon impact with the substrate when a molten droplet flattens, adheres, and solidifies. An increase in temperature causes a reduction in the dynamic viscosity of droplets; this, as well as the higher collision speed of droplets, leads to a higher degree of flattening on the surface [4,5]. Therefore, increasing the velocity and temperature of the in-flight particle leads to a denser coating formation, as well as good adhesion between the coating and the substrate [6].

Process control and optimization are essential to fulfill the requirements of the actual application [7,8]. The coating structure heavily depends on the melting degree of ceramic particles in the plasma and their impact velocity; therefore, understanding in-flight particle temperature and velocity is essential to obtain the desired coating performance [9]. In general, insufficient particle melting and low speed at impact lead to high porosity levels and poor intersplat bonding [4–8,10,11]. The mechanical properties of plasma-sprayed ceramic coatings depend on their microstructure. The micromechanical integrity of plasma-sprayed ceramic coatings is determined by features such as horizontal and vertical microcrack density, porosity, and lamellar or splat dimensions [12]. Since alumina is chemically stable, wear-resistant, and hard even at elevated temperatures, alumina is used as a base for high-performance ceramic coatings [13]. While sintered alumina contains the α-Al_2O_3 phase, the plasma-sprayed alumina coatings are composed of metastable γ-Al_2O_3 and stable α-Al_2O_3 phases. γ-Al_2O_3 phase occurs via fully or partly molten particles during plasma spray due to lower interfacial energy than the α-Al_2O_3 phase. The α-Al_2O_3 alumina phase tends to grow from the unmolten cores that are maintained by the bigger semi-molten particles [14], while the metastable γ-Al_2O_3 phase tends to nucleate from fully molten particles, since liquid-to-gamma transformation involves low interfacial energy [15]. V. C Misra et al. [13] demonstrated that the increase in plasma input power from 12 to 20 kW reduced the porosity of Al_2O_3 coatings from 16 to 9% and increased the amount of metastable γ-Al_2O_3 phase in as-sprayed alumina coatings. R. A. Abbas et al. [16] observed that the surface roughness increased as spray distance increased from 70 to 130 mm. Plasma torch power is considered to be one of the most effective ways to increase the velocity and temperature of the plasma jet. To understand the influence of plasma torch power on the characteristics of in-flight particles, there are already studies focusing on interactions between particles and plasma jet, such as the particle acceleration, heating up, melting, and re-solidification processes [2,6,17–21]. The majority of the research on plasma-sprayed coatings has been conducted using argon or nitrogen as a primary gas. Less information is obtained when oxygen is used as plasma-forming gas. D. Zois et al. [22] demonstrated that an increase in the torch power increased the γ-Al_2O_3 phase content in air-sprayed alumina coatings. The phase composition is strongly related to the type and nature of the used feedstock powders. This work introduces a visualization method to analyze plasma-sprayed particles' movement using high-speed video camera footage. In previous works, other authors analyzed flame spray pyrolysis [23], and plasma jet instabilities and fluctuations [24,25], observed using high-speed cameras; the results of a single particle motion are still lacking in the scientific literature.

Meanwhile, detailed information about the application of air as the primary gas for the deposition of alumina coatings by plasma spraying and the relationship between the plasma temperature and phase composition of produced Al_2O_3 coatings is insufficient. Therefore, in this research, air was selected as a primary gas to simplify this technique, and make it more economical; it addition, it was selected to provide a wider understanding of the influence of plasma torch power on plasma jet temperature, particle velocity, substrate temperature, and the effect of these parameters on the surface morphology and phase composition of as-sprayed alumina coatings.

2. Materials and Methods

Using a direct-current (DC) plasma torch developed at the Lithuanian Energy Institute (Kaunas, Lithuania), Al_2O_3 coatings were applied to steel (P265GH) substrate at atmospheric pressure [26,27].

The steel substrate samples (with dimensions of 40 mm $\times$ 10 mm $\times$ 6 mm) were chemically cleaned to improve the surface roughness and remove impurities. Air was used as the primary plasma generating medium and powder carrier gas. In order to raise the temperature of the plasma jet, hydrogen was also added as a secondary gas.

The water-cooled sample holder held the substrates, and the deposition process took around 60 s. Air was used as the primary gas (flow rate of 3.7 g/s), hydrogen was used as

the secondary gas (flow rate of 0.06 g/s), and air served as the particle carrier gas (flow rate of 0.75 g/s). The spraying distance was kept at 70 mm. Conventional 64 µm Al_2O_3 (MOGUL PC15, purity 99.8%, MOGUL METALLIZING GmbH, Kottingrunn, Austria) powders were used as a feedstock material injected into the plasma torch nozzle (internal diameter of 7 mm). Before the coating deposition process, the powders were dried for 12 h at 473 K to remove any moisture that may have accumulated during storage. An additional sub-layer from aluminum powders was deposited using the same plasma spray technique just before the coating layer, to improve the adhesion of the coating. Coatings were formed using five different power modes: 29.4, 33.6, 37.8, 42.0, and 45.1 kW. The surface morphology of coatings was analyzed via scanning electron microscopy using a Hitachi S-3400N (SEM, Hitachi, Tokyo, Japan). The elemental composition measurements were performed from a 1.05 mm^2 surface area at 4 different points for each sample via energy-dispersive X-ray spectroscopy D8 Discover X-ray diffractometer (Bruker ASX GmbH, Billerica, MA, USA). The phase composition was determined via X-ray diffraction (XRD) using Bruker D8 equipment (Bruker, Hamburg, Germany) with CuKα (λ = 0.154059 nm) radiation (2θ in the range from 20 to 70°). The mean square surface roughness (R_q) was measured using the AMBIOS XP-200 profilometer (Ambios Technology Inc., Santa Cruz, CA, USA). The velocity of in-flight particles was determined by analyzing the slow-motion footage, captured by a high-speed camera (Phantom Miro M310, Wayne, NJ, USA) during the plasma spray. A fast, 12-bit, 25.6 mm × 16.0 mm CMOS sensor camera equipped with a zoom lens and a neutral UV filter was used to visualize the plasma spray. Finally, the temperature of the steel surface was measured by connecting a type-K thermocouple to the bottom side of the steel. The temperature in the centerline of the plasma flow at a distance of 70 mm from the exit nozzle was measured using a type-B (platinum/rhodium) thermocouple.

3. Results and Discussion

The temperature and velocity of the plasma jet heavily depend on the input power of the plasma torch. At an initial input power of 29.4 kW, the mean temperature of the plasma jet at the nozzle exit was 3380 K (Figure 1), and upon increasing the input power to 33.6 kW, the plasma jet temperature increased to 3470 K. A further increase in power to 37.8 and 42.0 kW had a similar effect and increased the plasma jet temperature to 3520 K and 3610 K, respectively. The highest temperature of 3680 K was achieved with an input power of 45.1 kW, due to the increased density of the arc column under constant voltage [28]. The plasma jet temperature was also measured in the central part of the plasma flow at the coating's deposition distance (70 mm). The lowest temperature of 1730 K was observed at the lowest torch power (29.4 kW). The temperature of the plasma flow increased from 1730 to 2090 K (a difference of 360 K) with the enhancement of the torch power (Table 1).

Table 1. Summary of plasma jet operational settings.

I, A	P, kW	T_1, K	T_2, K	T_3, K	V_1, m/s	V_2, m/s
140	29.4	3380 ± 25	1730 ± 25	870 ± 20	965 ± 10	380 ± 50
160	33.6	3470 ± 25	1880 ± 25	915 ± 20	995 ± 10	390 ± 50
180	37.8	3520 ± 25	1930 ± 25	970 ± 20	1010 ± 10	400 ± 50
200	42.0	3610 ± 25	2010 ± 25	1010 ± 20	1040 ± 10	420 ± 50
220	45.1	3680 ± 25	2090 ± 25	1050 ± 20	1060 ± 10	450 ± 50

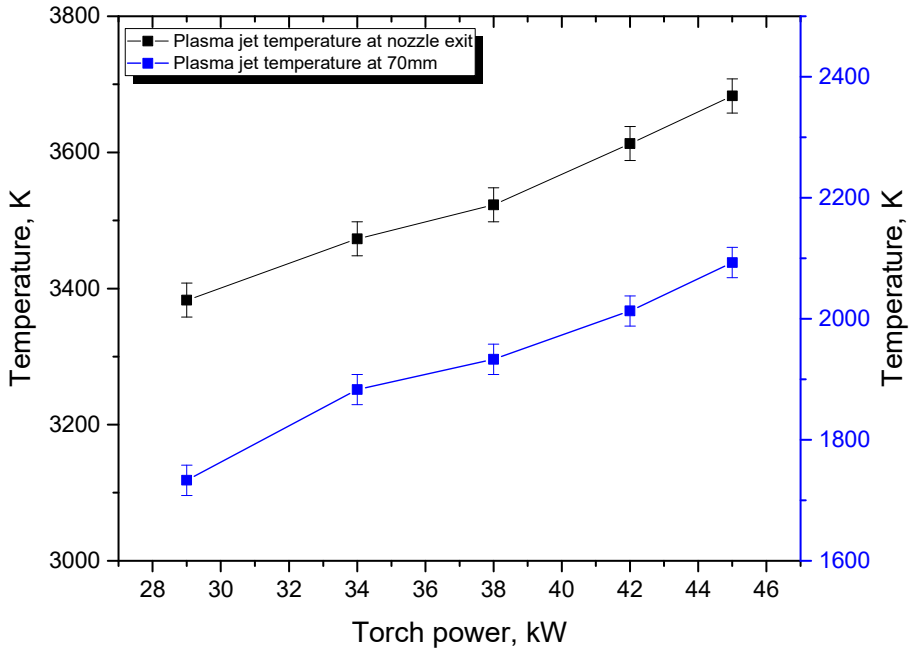

Figure 1. Plasma jet temperature at the nozzle exit and at a distance of 70 mm as a function of input power.

A similar tendency can be observed with the plasma jet velocity (Figure 2). The velocity of the plasma jet gradually increases along the axial direction from 965 m/s at 29.4 kW to 1060 m/s at 45.1 kW input power. This could be explained by the fact that the velocity of the plasma jet is strongly temperature-dependent, and it increases with an increasing arc current [28,29].

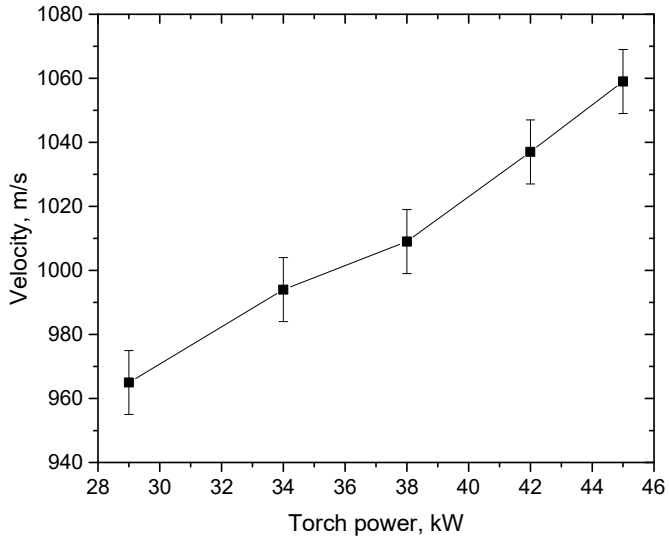

Figure 2. Plasma jet velocity as a function of input power.

The velocity of alumina particles was calculated by analyzing video footage of plasma spray, captured by a high-speed camera at 60,000 frames per second with 16 µs exposure time, using ImageJ software. Figure 3 shows two different frames used in calculating the velocity of in-flight Al_2O_3 particles. The velocity was calculated by measuring the distance that one particle travels between two frames. At least 10 particles were tracked for every power setting, and the mean velocity values were calculated (Table 1). The lowest velocity of the sprayed particle is observed at 29.4 kW of torch power. It gradually increases with the increase in plasma torch power, because the plasma jet accelerates the alumina powders towards the sample. Therefore, a higher velocity of particles is accelerated by a

relatively higher velocity of the plasma jet. The highest velocity of particles (450 ± 50 m/s) is recorded when the power of the plasma torch and the rate of the plasma jet is the highest. The results indicate that by increasing plasma torch power from 29.4 to 45.1 kW, in-flight particle velocity is enhanced by 70 m/s. M. Cuglietta et al. [29] demonstrated that the velocity of Samaria-doped ceria feedstock particles could be enhanced with an increase in input power or gas feed rate. A summary of the plasma jet operational settings is given in Table 1, where P is the plasma torch power; T_1 is the plasma jet temperature at the nozzle exit; T_2 is the plasma jet temperature at 70 mm distance; T_3 is the steel surface temperature during plasma spraying; V_1 is the plasma jet velocity; and V_2 is the in-flight alumina particle velocity.

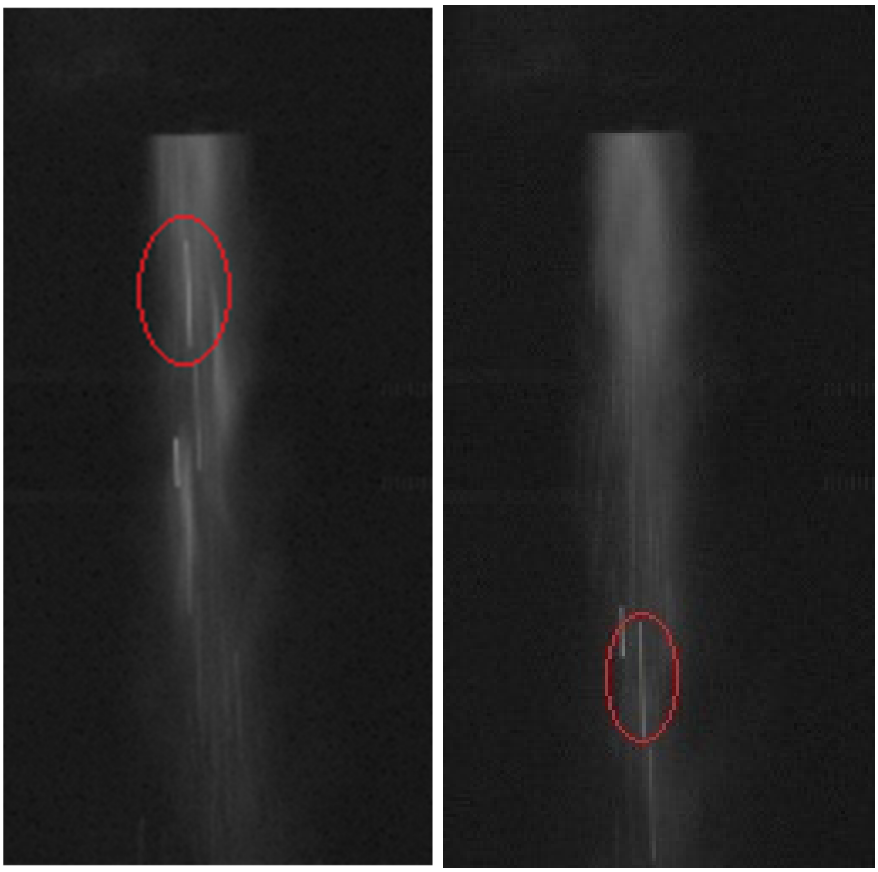

(**a**) (**b**)

Figure 3. A frame of video footage at (**a**) 1.314811 s and (**b**) 1.314862 s.

Figure 4 shows the temperature of the steel surface during the coating process. As can be seen from the graph, the temperature increases gradually over time and starts to stabilize towards the end of the spraying process, because the steel substrate was being cooled by water to avoid overheating. The temperature of the steel sample also increases with increasing torch power due to the higher plasma jet temperature (Figure 1). The results indicate that the steel surface temperature is almost two times lower compared to the plasma jet temperature at the same torch power values.

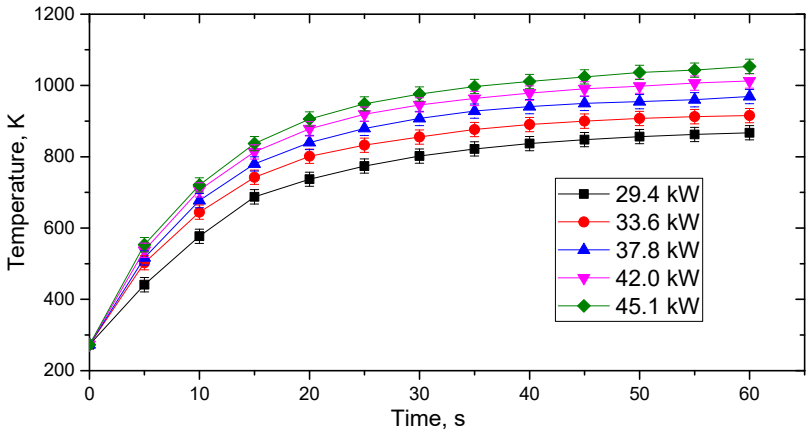

Figure 4. Sample temperature during the coating process.

Figure 5 presents the SEM view of the Al_2O_3 coatings using different plasma torch input power. The structure of all Al_2O_3 coatings is lamellar and quite similar, and the surface morphology of the coatings is typical for the plasma spray technique. However, there are slightly more unmolten particles on the surface of the Al_2O_3 coating (marked with red arrows) formed using lower spraying power (Figure 5a,b). With increased input power, the coating seems to become smoother, with fewer dips and peaks on the surface. There are no visible cracks or delamination zones on the sprayed Al_2O_3 coatings. Therefore, it can be stated that even using the 29.4 kW spraying power, powders were melted sufficiently enough. It should be noted that the molten state of the spraying feedstock particles was improved, and the number of fully melted Al_2O_3 particles was enhanced with an increase in torch power. The surface of the coating contained more melted areas with overlapped irregular splats (Figure 5e,f). Such phenomena are related, due to both the lower kinetic viscosity caused by higher temperature and larger kinetic energy for higher in-flight velocity, with the enhancement of power increasing from 29.4 to 45.1 kW [2,4,6].

The cross-sections of the coatings are shown in Figure 6. All deposited Al_2O_3 coatings demonstrated good adhesion to the steel substrate. There is a minimal number of microcracks and pores between the substrate and the coating; however, over the entire coating width, there are a lot more cavities, which are common for plasma-sprayed coatings [30,31]. The coating thickness was similar for all samples (around 40 µm).

The surface roughness of the samples was measured and analyzed using a profilometer, as shown in Table 2. The results indicate that the sample formed at 29.4 kW power has the roughest surface (R_q-7.13 µm). Input power gradually reduce the surface roughness and the smoothest surface is obtained using a power of 45.1 kW (R_q-5.54 µm) due to more particles being fully melted. Thus, the size of the pores decreases with increasing power of the plasma torch. A surface roughness reduction with torch power enhancement was obtained by several authors. V. C. Misra et al. [13] indicated that the surface roughness of alumina coatings was reduced from 9.24 to 7.02 µm when the input power was increased from 16 to 20 kW. The velocity and temperature of the plasma jet increased with the torch power. As a result, the temperature of the particles rose, and a higher degree of particle melting was obtained. Thus, the number of non-molten or semi-molten particles that reached the surface was reduced. The alumina surface is composed of a larger number of fully melted particles in the presence of a splat formation, resulting in lower surface roughness [9,13]. R. A. Abbas et al. [16] observed that the surface roughness increased with an increase in spray distance due to non-melted or insufficiently melted particles. T. Ghara et al. [9] observed that an increase in particle velocity from 197 to 219 m/s reduced the porosity and roughness values. However, a further increase in particle velocity increased the porosity and surface roughness of Al_2O_3 coatings [9]. Such a phenomenon was assigned to the splashing behavior of the splat at a higher velocity of feedstock particles [9,15]. Additionally,

at a higher temperature, the molten particles demonstrated lower viscosity values, and a less viscous liquid is more likely to splash [15].

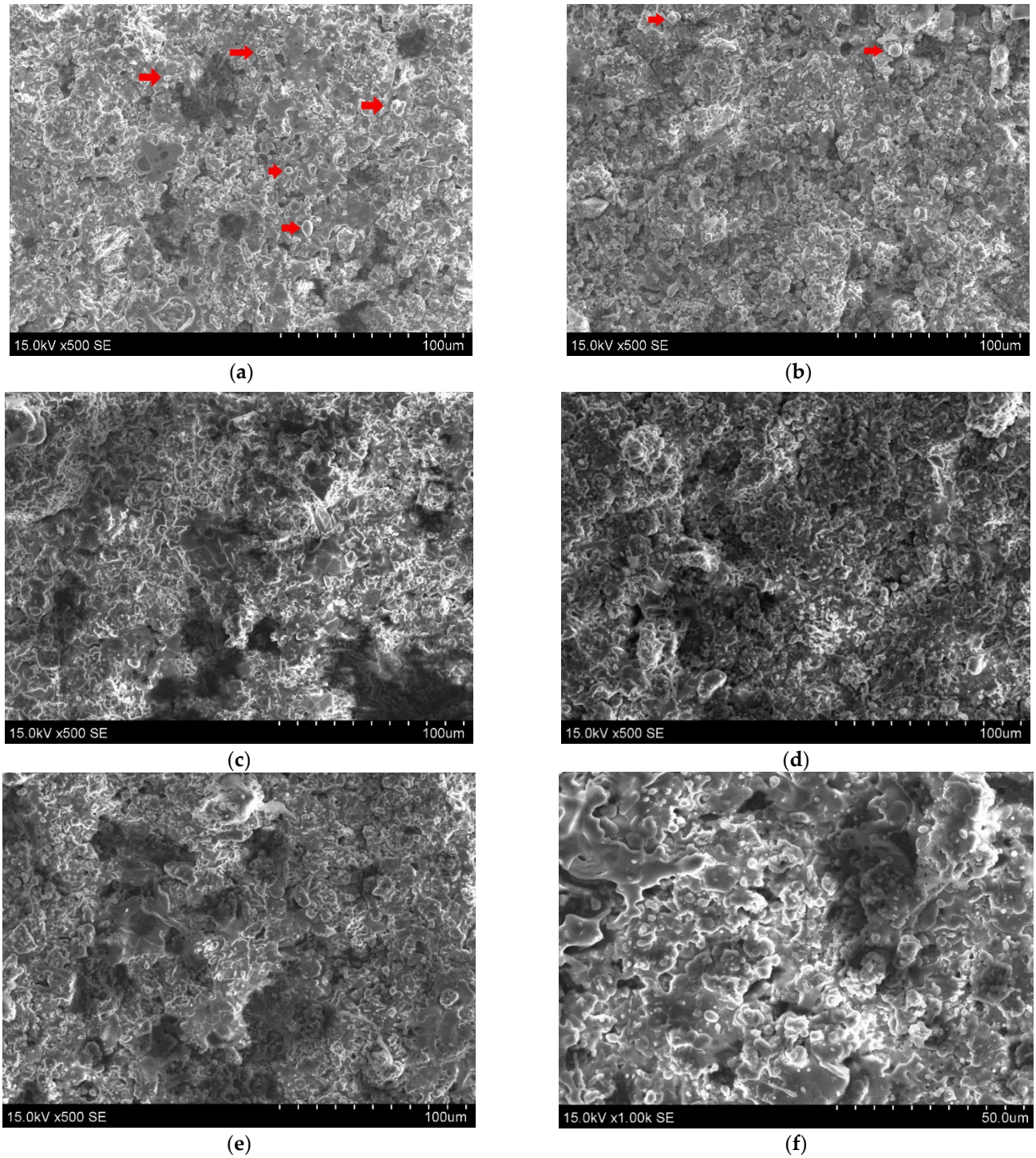

Figure 5. SEM micrographs of coating surface, using different plasma torch input powers: (**a**) 29.4 kW; (**b**) 33.6 kW; (**c**) 37.8 kW; (**d**) 42.0 kW; (**e**) 45.1 kW; and (**f**) 45.1 kW.

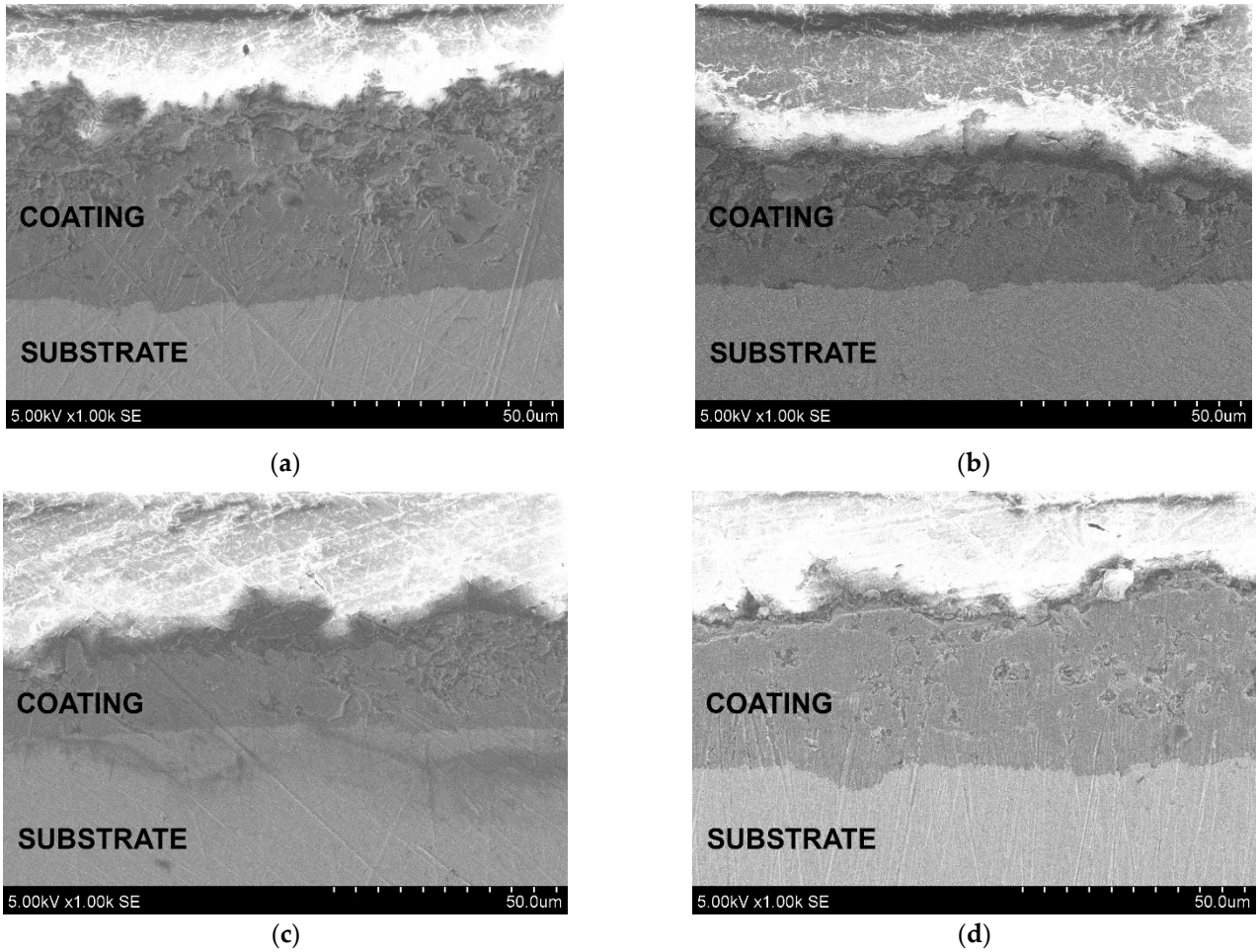

Figure 6. Cross-sections of coating surfaces using different plasma torch input powers: (**a**) 29.4 kW; (**b**) 33.6 kW; (**c**) 42.0 kW; and (**d**) 45.1.

Table 2. Elemental composition and mean square roughness of alumina coatings.

Torch Input Power, kW	Al, at.%	O, at.%	R_q, µm
29.4	38.7 ± 2	61.3 ± 2	7.13
33.6	38.9 ± 2	61.1 ± 2	6.73
37.8	38.5 ± 2	61.5 ± 2	6.34
42.0	38.4 ± 2	61.6 ± 2	5.97
45.1	38.8 ± 2	61.2 ± 2	5.54

Figure 7 shows the X-ray diffraction patterns of Al_2O_3 coatings, formed using different plasma torch input powers. The feedstock (Al_2O_3 MOGUL PC15) powders consist only of stable α-phase, while the coating is composed of stable alpha and metastable gamma phases. It is usually the case that there is a higher fraction of metastable phase because of the high cooling rate of molten material during the solidification process. Therefore, it shows the extent of the melting of in-flight particles [13,15]. In most coating samples, there are three aluminum peaks at 2θ = 38.5°, 44.8°, and 65.3°, that are attributed to the crystalline aluminum formed during the aluminum sub-layer deposition process. There are several peaks of the α-Al_2O_3 phase at 2θ = 25.6°, 35.2°, 43.4°, 52.6°, 57.6°, and 68.3°, and of the γ-Al_2O_3 phase at 2θ = 19.4°, 37.8°, 39.6°, 46.0°, 61.2°, and 67.0° [13,15,32]. The γ-Al_2O_3 phase in the coatings increases gradually with an increase in plasma torch power. This trend is attributed to the higher melting degree of alumina powders, since the gamma phase forms only when the alumina particles are fully melted in the plasma jet. This was also confirmed by S. Yugeswaran et al. [32] and C. J. Li et al. [6]. In their work, the authors also conclude

that the formation of the γ-Al_2O_3 phase is only possible via the fully melted alumina particles, since the powders consist of only the α-Al_2O_3 phase [33]. An improvement in γ-Al_2O_3 phase formation was also noticed by only increasing the plasma jet temperature [9] and by increasing the combined Critical Plasma Spray Parameter (CPSP) [34]. T. Ghara et al. [9] demonstrated that the γ-Al_2O_3 phase content increased from ~82% to 87% with an increase in Al_2O_3 particle temperature from 2590 to 2671 K. This was further confirmed when comparing the gamma-to-alpha alumina ratio of the two most intense peaks, α-Al_2O_3 at 43.4° and γ-Al_2O_3 at 46.0°. Using the lowest input power, 29.4 kW, the γ-Al_2O_3 / α-Al_2O_3 ratio was 1.64. The ratio decreases to 1.36 at 33.6 kW power. At 37.8 and 42.0 kW power, the ratio is the same—2.75. The highest gamma-to-alpha alumina peak intensity ratio of 5.11 is achieved using the highest power of 45.1 kW, whereas the melting degree of particle and substrate temperature, which directly affect the cooling rate of the melted alumina particles, are the main factors for the phase transition [6,9], [14,33]. It was determined that the substrate temperature is enhanced from 870 to 1050 K with an increase in torch power. However, the amount of γ-Al_2O_3 phase is further enhanced despite the higher substrate temperature. E.J. Yang et al. [35] determined that the phase structure of alumina splats varied from the amorphous phase through γ-Al_2O_3 (at 873 and 973 K) and to the α-Al_2O_3 phase with an increase in the substrate temperature from 573 to 1173 K. It was stated that at cooling rates in the range of 1–100 K/s, only α-Al_2O_3 forms in as-spayed alumina coatings [35]. Our research shows that even at a substrate temperature of ~1050 K (when the plasma jet temperature reaches ~2090 K) the required cooling rate for γ-Al_2O_3 nucleation is obtained and the content of the γ-Al_2O_3 phase is enhanced.

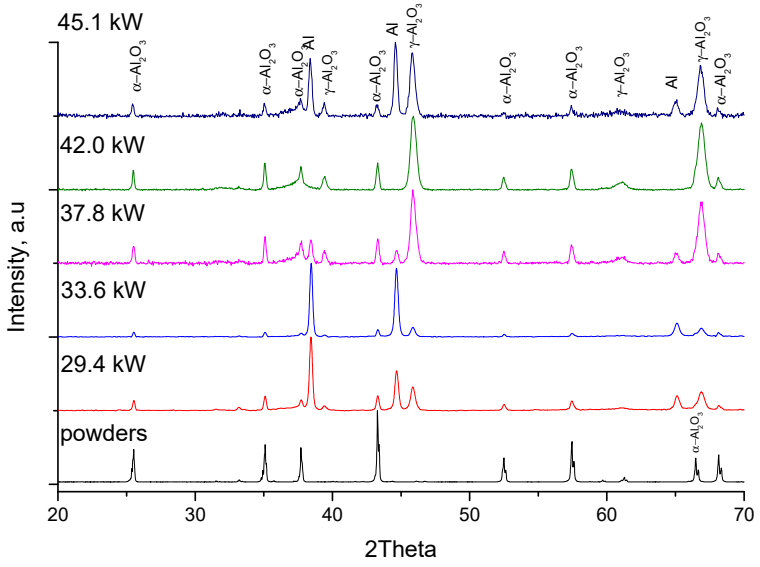

Figure 7. X-ray diffraction pattern of Al_2O_3 coatings formed using different plasma torch power parameters.

Table 2 shows the elemental composition of Al_2O_3 coatings. The changes in aluminum and oxygen rates are minimal. It should be noted that the Al concentration varies from 38.4 at.% to 38.9 at.%, while the amount of oxygen is in the range of 61.1–61.5 at.%. Therefore, it can be stated that plasma torch power did not influence the elemental composition of alumina coatings.

Figure 8 shows the cross-section mapping images of the Al_2O_3 coating formed using 45.1 kW torch power. The elemental distribution is similar for all plasma-sprayed Al_2O_3 coatings. The clear boundaries between the steel (red color), bonding aluminum layer (green color), and Al_2O_3 coating (mixed blue and green colors) can be seen in the cross-section views (Figure 8). Aluminum is more concentrated alongside the steel substrate, while oxygen is more prominent towards the outer layer of the coating, and some irregularities of the outer layer occur due to the cutting and polishing of the cross-section sample. However,

the most even distribution of oxygen over the entire width of the coating can be observed in the sample formed using a plasma torch power of 45.1 kW.

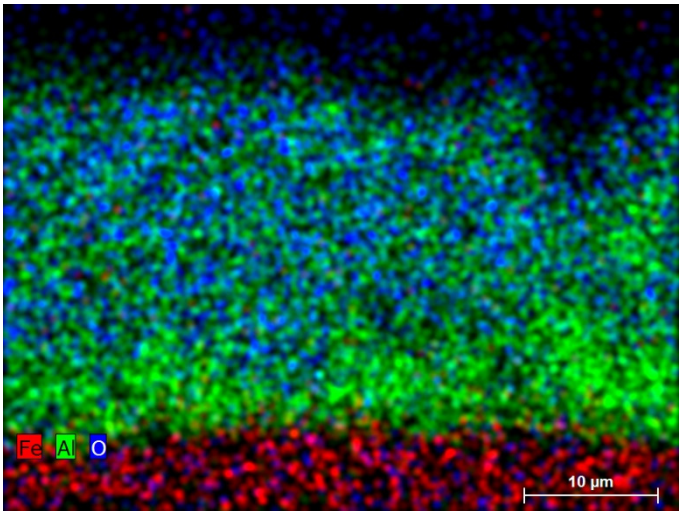

Figure 8. Elemental distribution maps of a cross-section of Al_2O_3 coatings formed using 45.1 kW power.

4. Conclusions

Alumina coatings were formed using atmospheric plasma spray, increasing torch power from 29.4 to 45.1 kW. The results indicate that an increase in the plasma torch power increased the temperature of the plasma jet from 3380 to 3680 K at the exit nozzle, and from 1730 to 2090 K at the sample holding distance. Consequently, the steel surface temperature increased from 870 to 1050 K. The plasma jet velocity increased from 965 to 1060 m/s, while in-flight particle speed increased from 380 to 450 m/s, with the enhancement of torch power. Variation in the plasma torch power did not affect the elemental composition of the coatings. The quantities of aluminum and oxygen were mainly the same, around 39 at.% and 61 at.%, respectively. The most even distribution of oxygen over the width of the coatings was observed using 45.1 kW of power. None of the formed coatings had visible cracks or delamination zones, since even the lowest power was enough to melt alumina powders sufficiently. An increase in plasma torch input power resulted in a decrease in the α-Al_2O_3 phase and an increase in γ-Al_2O_3, contributing to a higher melting degree of alumina powders. The phase ratio of γ-Al_2O_3/α-Al_2O_3 increased from 1.64 to 5.11 with an increase in plasma torch power from 29.4 to 45.1 kW. This also caused a reduction in surface roughness (R_q) from 7.13 to 5.54 µm.

Author Contributions: Conceptualization, A.Š., L.M. and V.G.; Data curation, A.Š.; Formal analysis, A.Š.; Funding acquisition, V.G.; Investigation, A.Š., R.K., R.U. and M.A.; Methodology, A.Š., R.K., R.U. and M.A.; Supervision, L.M. and V.G.; Visualization, A.Š.; Writing—original draft, A.Š.; Writing—review & editing, A.Š., L.M. and V.G. All authors have read and agreed to the published version of the manuscript.

Funding: This research received no external funding.

Institutional Review Board Statement: Not applicable.

Informed Consent Statement: Not applicable.

Data Availability Statement: The authors confirm that the data supporting the findings of this study are available within the article.

Acknowledgments: This research (Project No. 01.2.2-LMT-K-718-01-0069) was funded by the European Regional Development Fund according to the supported activity 'Research Projects Implemented by World-class Researcher Groups', under Measure No. 01.2.2-LMT-K-718.

Conflicts of Interest: The authors declare no conflict of interest.

References

1. Tamošiūnas, A.; Valatkevičius, P.; Gimžauskaitė, D.; Jeguirim, M.; Mėčius, V.; Aikas, M. Energy recovery from waste glycerol by utilizing thermal water vapor plasma. *Environ. Sci. Pollut. Res.* **2017**, *24*, 10030–10040. [CrossRef]
2. Lv, M.; Zhang, G.; Geng, H. Effect of spraying power on the microstructure and thermoelectric performance of plasma-sprayed higher manganese silicides films. *Surf. Coat. Technol.* **2019**, *363*, 152–160. [CrossRef]
3. Kavaliauskas, Ž.; Kėželis, R.; Milieška, M.; Marcinauskas, L.; Valinčius, V.; Aikas, M.; Uscila, R.; Baltušnikas, A.; Žunda, A. Influence of different plasma spraying methods on the physical properties of YSZ coatings. *Surf. Interfaces* **2021**, *24*, 101120. [CrossRef]
4. Fauchais, P.; Montavon, G. Plasma spraying: From plasma generation to coating structure. *Adv. Heat Transf.* **2007**, *40*, 205–344.
5. Sobhanverdi, R.; Akbari, A. Porosity and microstructural features of plasma-sprayed Yttria stabilized Zirconia thermal barrier coatings. *Ceram. Int.* **2015**, *41*, 14517–14528. [CrossRef]
6. Li, C.J.; Sun, B. Effects of spray parameters on the microstructure and property of Al_2O_3 coatings sprayed by a low power plasma torch with a novel hollow cathode. *Thin Solid Films* **2004**, *450*, 282–289. [CrossRef]
7. Friis, M.; Persson, C.; Wigren, J. Influence of particle in-flight characteristics on the microstructure of atmospheric plasma sprayed yttria stabilized ZrO_2. *Surf. Coat. Technol.* **2001**, *141*, 115–127. [CrossRef]
8. Zhu, J.; Wang, X.; Kou, L.; Zheng, L.; Zhang, H. Prediction of control parameters corresponding to in-flight particles in atmospheric plasma spray employing convolutional neural networks. *Surf. Coat. Technol.* **2020**, *394*, 125862. [CrossRef]
9. Ghara, T.; Bandyopadhyay, P.P. Understanding the role of in-flight particle temperature and velocity on the residual stress depth profile and other mechanical properties of atmospheric plasma sprayed Al_2O_3 coating. *J. Eur. Ceram. Soc.* **2022**, *42*, 4353–4368. [CrossRef]
10. Vaxevanidis, N.M.; Manolakos, D.E.; Petropoulos, G.P. Surface integrity and tribological behavior of plasma sprayed alumina coatings on steel and aluminum substrates. *Tribol. Ind.* **2004**, *26*, 42–47.
11. Bai, Y.; Zhao, L.; Qu, Y.; Fu, Q.; Wang, Y.; Liu, K.; Tang, J.; Li, B.; Han, Z. Particle in-flight behavior and its influence on the microstructure and properties of supersonic-atmospheric-plasma-sprayed nanostructured thermal barrier coatings. *J. Alloys Compd.* **2015**, *644*, 873–882. [CrossRef]
12. Erickson, L.C.; Hawthorne, H.M.; Troczynski, T. Correlations between microstructural parameters, micromechanical properties and wear resistance of plasma sprayed ceramic coatings. *Wear* **2001**, *250*, 569–575. [CrossRef]
13. Misra, V.C.; Chakravarthy, Y.; Khare, N.; Singh, K.; Ghorui, S. Strongly adherent Al_2O_3 coating on SS 316L: Optimization of plasma spray parameters and investigation of unique wear resistance behaviour under air and nitrogen environment. *Ceram. Int.* **2020**, *46*, 8658–8668. [CrossRef]
14. Zamani, P.; Valefi, Z. Microstructure, phase composition and mechanical properties of plasma sprayed Al_2O_3, Cr_2O_3 and Cr_2O_3-Al_2O_3 composite coatings. *Surf. Coat. Technol.* **2017**, *316*, 138–145. [CrossRef]
15. Sabiruddin, K.; Joardar, J.; Bandyopadhyay, P.P. Analysis of phase transformation in plasma sprayed alumina coatings using Rietveld refinement. *Surf. Coat. Technol.* **2010**, *204*, 3248–3253. [CrossRef]
16. Abbas, R.A.; Ajeel, S.A.; Bash, M.A.A.; Kadhim, M.J. Effect of plasma spray distance on the features and hardness reliability of YSZ thermal barrier coating. *Mater. Today Proc.* **2021**, *42*, 2553–2560. [CrossRef]
17. Caliari, F.R.; Miranda, F.S.; Reis, D.A.P.; Filho, G.P.; Charakhovski, L.I.; Essiptchouk, A. Plasma torch for supersonic plasma spray at atmospheric pressure. *J. Mater. Process. Technol.* **2016**, *237*, 351–360. [CrossRef]
18. Xiong, H.B.; Zheng, L.L.; Li, L.; Vaidya, A. Melting and oxidation behavior of in-flight particles in plasma spray process. *Int. J. Heat Mass Transf.* **2005**, *48*, 5121–5133. [CrossRef]
19. Zhang, D.; Zheng, L.; Hu, X.; Zhang, H. Numerical studies of arc plasma generation in single cathode and three-cathode plasma torch and its impact on plasma spraying. *Int. J. Heat Mass Transf.* **2016**, *98*, 508–522. [CrossRef]
20. Gao, Y.; Xu, X.; Yan, Z.; Xin, G. High hardness alumina coatings prepared by low power plasma spraying. *Surf. Coat. Technol.* **2002**, *154*, 189–193. [CrossRef]
21. Marcinauskas, L. Deposition of alumina coatings from nanopowders by plasma spraying. *Medziagotyra* **2010**, *16*, 47–51.
22. Zois, D.; Lekatou, A.; Vardavoulias, M.; Vazdirvanidis, A. Nanostructured alumina coatings manufactured by air plasma spraying: Correlation of properties with the raw powder microstructure. *J. Alloys Compd.* **2010**, *495*, 611–616. [CrossRef]
23. Meierhofer, F.; Hodapp, M.; Achelis, L.; Buss, L.; Noriler, D.; Meier, H.F.; Fritsching, U. Investigation of atomization concepts for large-scale flame spray pyrolysis (FSP). *Mater. Und Werkst.* **2014**, *45*, 765–778. [CrossRef]
24. Bobzin, K.; Ote, M.; Knoch, M.A.; Alkhasli, I.; Heinemann, H. High-Speed Video Analysis of the Process Stability in Plasma Spraying. *J. Therm. Spray Technol.* **2021**, *30*, 987–1000. [CrossRef]
25. Bobzin, K.; Heinemann, H.; O'Brien, A. Capturing the Influence of Jet Fluctuations on Particles in Plasma Spraying. *J. Therm. Spray Technol.* **2022**, *31*, 59–69. [CrossRef]
26. Šuopys, A.; Marcinauskas, L.; Grigaitienė, V.; Kėželis, R.; Aikas, M.; Uscila, R.; Tučkutė, S.; Lelis, M. The effect of heat treatment on the microstructure and phase composition of plasma sprayed Al_2O_3 and Al_2O_3-TiO_2 coatings for applications in biomass firing plants. *Coatings* **2021**, *11*, 1289. [CrossRef]
27. Brinkiene, K.; Kezelis, R. Effect of alumina addition on the microstructure of plasma sprayed YSZ. *J. Eur. Ceram. Soc.* **2005**, *25*, 2181–2184. [CrossRef]

28. Li, Q.; Hu, J.; Xie, J.; Wang, X.; Yu, C.; Jiang, S.; Liu, Z.; Jiang, X.; Sun, C.; Li, E.; et al. Effect of spray process on dielectric properties of APS-deposited CaO–B_2O_3–SiO_2 glass-ceramic coatings. *J. Eur. Ceram. Soc.* **2020**, *40*, 4527–4535. [CrossRef]
29. Cuglietta, M.; Kesler, O. Relationship between particle and plasma properties and coating characteristics of samaria-doped ceria prepared by atmospheric plasma spraying for use in solid oxide fuel cells. *J. Therm. Spray Technol.* **2012**, *21*, 448–460. [CrossRef]
30. Fauchais, P.; Vardelle, A. Thermal Spray Coatings. In *Wiley Encyclopedia of Electrical and Electronics Engineering*; John Wiley & Sons, Inc.: Hoboken, NJ, USA, 2007.
31. Muhammad, M.M.; Jalar, A.; Shamsudin, R.; Isa, M.C. Effect of plasma spray parameters on porosity of fly ash deposited coatings. *AIP Conf. Proc.* **2014**, *1614*, 116–121.
32. Yugeswaran, S.; Selvarajan, V.; Vijay, M.; Ananthapadmanabhan, P.V.; Sreekumar, K.P. Influence of critical plasma spraying parameter (CPSP) on plasma sprayed Alumina-Titania composite coatings. *Ceram. Int.* **2010**, *36*, 141–149. [CrossRef]
33. Jiang, X.-Y.; Hu, J.; Jiang, S.-L.; Wang, X.; Zhang, L.-B.; Li, Q.; Lu, H.-P.; Yin, L.-J.; Xie, J.-L.; Deng, L.-J. Effect of high-enthalpy atmospheric plasma spraying parameters on the mechanical and wear resistant properties of alumina ceramic coatings. *Surf. Coat. Technol.* **2021**, *418*, 127193. [CrossRef]
34. Zhao, D.; Luo, F.; Zhou, W.; Zhu, D. Effect of critical plasma spray parameter on complex permittivity and microstructure by plasma spraying Cr/Al2O3 coatings. *Appl. Surf. Sci.* **2013**, *264*, 545–551. [CrossRef]
35. Yang, E.-J.; Luo, X.-T.; Yang, G.; Li, C.-J.; Takahashi, M.; Kuroda, S.; Kim, K. Impact of deposition temperature on crystalline structure of plasma-sprayed Al_2O_3 splats revealed by FIB-HRTEM technique. *Ceram. Int.* **2016**, *42*, 853–860. [CrossRef]